Dependency of Sliding Friction for Two Dimensional Systems on Electronegativity

Jianjun Wang
Avinash Tiwari
PGI-1, FZ Jülich, Germany
Yang Huang
Zhengzhou University
Bo Persson
IFF-Juelich
Yu Jia (jiayu@zzu.edu.cn)
Zhengzhou University

Article

Keywords: electronegativity, low dimensional systems, nanoscale devices, DFT

Posted Date: September 3rd, 2021

DOI: https://doi.org/10.21203/rs.3.rs-864954/v1

Dependency of Sliding Friction for Two Dimensional Systems on Electronegativity

Jianjun Wang[a,b,d], Avinash Tiwari[d], Yang Huang [b], Yu Jia[b, c,*], Bo N. J. Persson[d]

[a] *College of Science, Zhongyuan University of Technology, Zhengzhou, Henan 450007, China*

[b]*Key Laboratory for Special Functional Materials of Ministry of Education, and School of Materials Science and Engineering, Henan University, Kaifeng, Henan 475004, China*

[c]*International Laboratory for Quantum Functional Materials of Henan, and School of Physics, Zhengzhou University, Zhengzhou, Henan 450001, China*

[d]*PGI-1, FZ-Juelich, Germany, EU*

Abstract

We study the role of electronegativity in sliding friction for five different two-dimensional (2D) monolayer systems using ab-initio calculations within density functional theory (DFT) with van der Waals (vdW) corrections. We show that the friction depends strongly on the involved atoms' electronegativity difference. All the studied systems exhibit almost the same magnitude of the friction force when sliding along the nonpolar path, independent of the material and the surface structures. In contrast, for sliding friction along a polar path, the friction force obeys a universal linear scaling law where the friction force is proportional to atoms electronegativity difference of its constituent atoms. We show that atomic dipoles in the 2D monolayers, induced by the electronegativity difference, enhance the corrugation of the charge distribution and increase the sliding barriers accordingly. Our studies reveal that electronegativity plays an important role in friction of low dimensional systems, and provides a strategy for designing nanoscale devices.

* jiayu@zzu.edu.cn (Y Jia)

Understanding the origin of atom-scale friction, and controlling it when designing nanotechnological devices, pose a major challenge due to the intricate interfacial interaction [1-2]. Two-dimensional (2D) layered materials, such as graphene, hexagonal boron nitride (*h*-BN), and hexagonal molybdenum disulfide (MoS_2), due to their strong intralayer chemical bonding compared with the weak interlayer physical adsorption interaction, can serve as solid lubricants to minimize friction and wear in many applications [3-5]. Moreover, 2D layered structures often have novel electronic properties widely researched in the literature, which can further our understanding of their tribological behavior [6-9].

Friction is ultimately governed by the atomistic interactions determined by quantum mechanics [1, 2, 9]. Several studies have demonstrated that electronic structure and charge distribution are closely related to the friction behavior of low-dimensional system [5, 7-10]. Electronegativity difference among the constituent atoms is closely related to the friction in low-dimensional materials [11-17]. Experiments have shown that the sliding friction in insulating multiwall boron nitride nanotube (BNNT) is orders of magnitude stronger than that of semimetallic carbon nanotube, which were attributed to an increased potential barrier caused by the charge localization induced by the electronegativity difference between the boron and nitrogen atoms in BNNT [12]. This localization effect increases the corrugation amplitude of the interfacial potential. Similarly, *ab*-initio molecular dynamics simulation showed that the coefficient of friction (COF) of liquid water sliding on *h*-BN is about three times larger than that of graphene, which was ascribed to the greater corrugation of the energy landscape of *h*-BN [13].

From DFT calculations, it was found that the vdW interaction determines the interlayer binding, and the electrostatic interaction influences the sliding barrier for *h*-BN sliding on *h*-BN [14]. Hod speculated that a highly anisotropic interfacial friction should exist for the *h*-BN bilayer [15]. Gao shows that the contributions of electrostatic and dispersive interactions to the sliding energy profile are different in bilayers graphene and *h*-BN [16]. These results presented above confirm that the polarity plays an important role in friction for low dimensional systems. However, no study showing a clear connection between polarity and friction properties has been established.

In this study, the *ab*-initio calculations were carried out to investigate the role of electronegativity on friction in 2D systems [18-24]. We find that when two monolayers slide relative

to each other, the atom electronegativity difference along the sliding path strongly influences the interfacial friction properties, that is, the friction scales linearly with electronegativity difference in the sliding path.

Results

In order to study the influence of polarity on friction, we first discuss the sliding paths polarity character. Fig. 1(a) shows a schematic diagram of the sliding interface between two monolayers. The atoms A, B from the upper layer, and C, D from the bottom layer are arranged alternating along the sliding direction. We define the sliding systems total polarity along the sliding direction as the sum of the polarity of each single layer in that direction, which is decided by the electronegativity differences between A, B atoms, and C, D atoms. Here, the *h*-BN bilayer is chosen as an example to illustrate the polarity differences in different paths (see Fig. 1(b)). The most stable AA′ stacking (where B eclipsed N atoms) was chosen as an initial structure [14, 15, 25], and two highly symmetric directions were chosen as sliding paths. From the Fig. 1(b), we can see that there is only one kind of B (N) atom in the upper (bottom) layer along path I, and so the polarity is zero along this direction. However, B and N atoms are alternately arranged in the upper and the bottom layers along path II, which gives rise to in-plane dipoles in both the layers. Therefore, we denote path I as non-polar and path II as polar paths. The static friction is determined by the magnitude of the potential barrier along the sliding path [26-28]. Thus, depending on the sliding paths, different static friction values could be obtained [9, 29, 30]. In the *h*-BN bilayer case, the sliding paths with maximum polarity, and with non-polarity, are chosen to understand the relationship between electronegativity and friction. It also should be noted that the friction calculated is the static (or break-loose) friction force. However, if it is assumed that all the energy needed to reach the top of the energy barrier is dissipated before climbing the next barrier, the presented calculations also give information about the kinetic friction [31].

The optimized lattice parameters of graphene, *h*-BN, and MoS_2 are 2.47, 2.51, and 3.18 Å, respectively. Using these lattice parameters, the most stable bilayer stacking was obtained (see Tables S1 and S2 in Supporting Information (SI))), and is supported by other studies [14-16, 32-39]. Two sheets of the 2D monolayer were moved relative to each other along paths I and II to simulate the sliding process (see Figs. 1(b) and Fig. S1). The COF, as a function of the load is calculated, and

shown in Figs. 1(c)-(g). For the identical pristine bilayers, the COFs fall in a range of 0.07-0.2, which agrees with earlier studies [4, 8]. Among these systems, the non-polar graphene/graphene system (Fig. 1(c)) exhibits isotropic friction behavior. However, in the polar *h*-BN/*h*-BN (Fig. 1(d)) and MoS_2/MoS_2 (Fig. 1(e)) systems, the COF exhibit anisotropic behavior, in which the COF along the polar path II is almost two times larger than for the non-polar path.

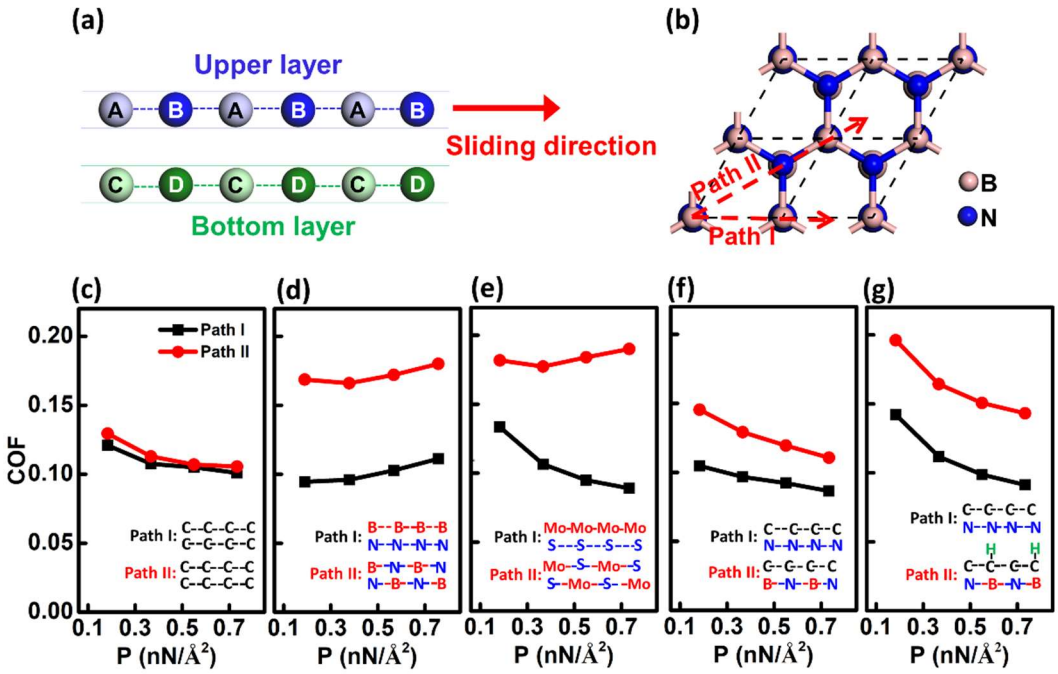

Fig. 1. Sliding model and friction characteristics. (a) General atomic arrangement of a sliding interface along the sliding direction. (b) Two sliding paths illustrated by *h*-BN/*h*-BN system with AA′ stacking as an example. Coefficient of friction as a function of normal pressure along polar and non-polar paths for (c) graphene/graphene (d) *h*-BN/*h*-BN (e) MoS_2/MoS_2 (f) graphene/*h*-BN and (g) H-graphene/*h*-BN systems.

We have examined the effect of electronegativity on the frictional properties for different sliding paths and found that the friction along a polar path is larger than that a non-polar path (see Fig. S2 in SI). Even for the minimum potential barrier path (a zigzag path), the friction of polar bilayer *h*-BN is still larger than that for the non-polar graphene system (see Fig. S3), showing that polarity plays an important part in the friction between two polar planes.

We next investigated the friction between polar and non-polar sheets using the interface of graphene sliding on *h*-BN (graphene/*h*-BN, see Fig. S1(b)). The computational model was simplified by enlarging the lattice constant of graphene to be equal to that of *h*-BN so that a

commensurate interface could be formed. Although the upper layer is non-polar, path II is still polar due to dipoles in the bottom layer along the sliding path (Fig. 1(f)). Like the polar/polar interface, the COF in the non-polar/polar system is also anisotropic. Again, it indicates that the polarity still has a significantly influence on friction even if dipoles exist only in one layer of the sliding interface.

Based on the graphene/*h*-BN system, we further consider the friction modulation by tuning the polarity of graphene. For this purpose, we induced polarity in the graphene lattice by single-side half hydrogenation (H-graphene, Fig. S1(c)). The covalent C-C bond in graphene turns into a partially ionic bond in H-graphene, with the charge transfer of 0.35 e. The COF between H-graphene and *h*-BN (H-graphene/*h*-BN) was calculated and is shown in Fig. 1(g). It is apparent that the COF along polar path II is larger than that of the non-polar path I. More importantly, the H-graphene/*h*-BN system has a larger COF than that of the graphene/*h*-BN and is consistent with the increase of the polarity induced by hydrogenation passivation. These calculations provide new insight on how to modify friction by surface modification.

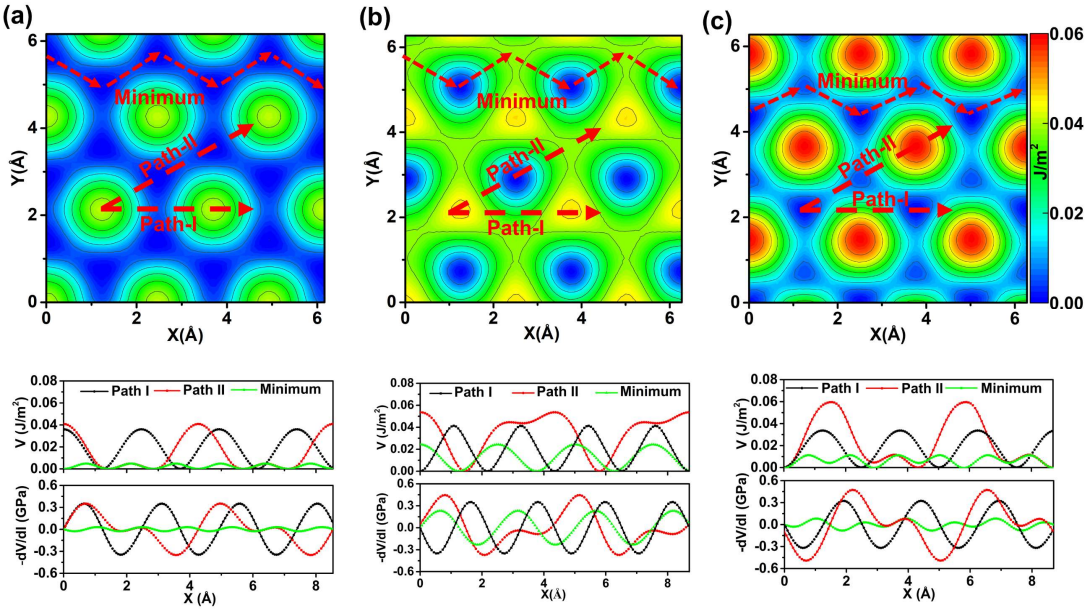

Fig. 2. Potential energy surfaces (PES). (a) graphene/graphene, (b) graphene/*h*-BN and (c) *h*-BN/*h*-BN systems. The minimum is taken as a reference. The corresponding potential barrier and friction forces along the three paths are plotted under each PES.

The variation of the binding energy as a function of the relative lateral position of the two surfaces in contact is denoted as the potential energy surface (PES) [24]. The corrugation of the PES

determines the intrinsic resistance to sliding and indicates of the maximum energy that can be dissipated during frictional processes. In this calculation, the atoms at each stacking are allowed to fully relax along vertical direction and so we construct an actual PES at zero pressure. To do this, three typical systems are chose to represent the non-polar/non-polar, non-polar/polar and polar/polar cases, namely, graphene/graphene, graphene/*h*-BN and *h*-BN/*h*-BN, respectively. The calculated PESs are shown in Fig. 2. We can see that the corrugation of the PES is strongly dependent on polarity of sliding paths, whereas *h*-BN/*h*-BN system sliding along path II possesses the largest corrugation (Fig. 2(c)), and the graphene/graphene system the smallest one (Fig. 2(a)). The magnitude of saddle point interaction energy and the maximum corrugation amplitude of the PES for graphene/graphene and *h*-BN/*h*-BN systems can be found in Tables S1 and S2. To examine the difference of the sliding path on friction, we plotted the potential profiles along the two paths, as indicated in middle of Fig. 2. In the graphene/graphene system, of course, they exhibit the same potential energy corrugation. However, for the graphene/*h*-BN and *h*-BN/*h*-BN systems, the corrugation along path II is much larger than that of path I. The lateral forces acting on the slider dragged along the two paths were also calculated and are shown in Fig. 2 (bottom). In all, the anisotropic friction behavior for the polar system [14] is blindingly obvious, which corroborates the results in Fig. 1.

In addition, the majority view is that the real sliding path between neighbor minima at static friction occurs near saddle points of PES. The sliding barrier and friction force along the minimum potential energy path (zigzag path, see Figs. 2 and S3) indicate that even for the zigzag path polarity still plays an important role in friction for the *h*-BN/*h*-BN bilayer. We also calculated the PESs for the other two systems, which also exhibit larger friction along the polar path (see Fig. S4).

From the above calculations, we conclude that the frictional properties exhibited by 2D systems both with and without external load depend on the polarity and hence on the sliding direction. The sliding potential barrier $\Delta V = \Delta E + F_N \Delta h$, where F_N is the external load, ΔE and Δh are the changes in the binding energy and the interlayer separation during sliding, respectively [23]. Note that ΔV depends on (a) the variation of the adsorption bond energy ΔE, and (b) the work done $F_N \Delta h$ to overcome the Δh during sliding. When no external load is applied, the friction is

determined by the ΔE. However, for the normal loads used in our study, the most important contribution to the sliding barrier comes from the work done against the external force (see Fig. S5).

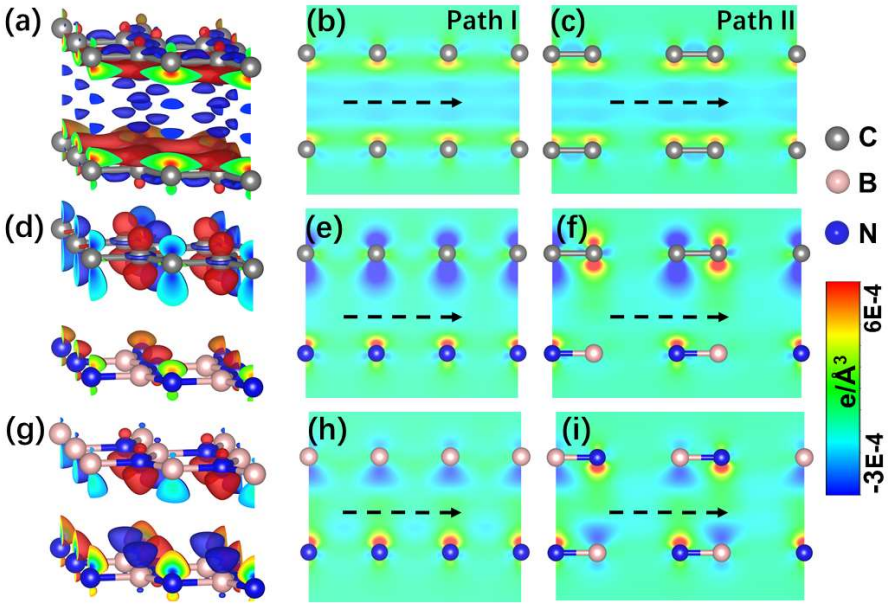

Fig. 3. The charge density difference information. (a) The charge density difference of bilayer graphene, with an isosurface charge density of 0.0003 electrons/Å^3. The red and blue indicating charge accumulation and depletion regions, respectively and the dotted arrow lines indicate sliding direction. The corresponding cross-sectional views of the bilayer system along (b) path I and (c) path II. (d-f) the case of graphene/*h*-BN system and (g-i) the case of *h*-BN/*h*-BN system.

The relationship between friction and polarity could be obtained by examining the roughness of charge distribution along different sliding paths. To understand the origin of the anisotropic friction behavior, we calculated the charge density difference of these 2D systems. First, from Fig. 3(a)-(c) for the graphene /graphene system, the charge distribution between the two graphene layers is uniform and flat along the sliding paths, which corresponds to a small charge corrugation and sliding barrier. Then, for the polar bilayer systems of graphene/*h*-BN (Figs. 3(d)-(f)) and *h*-BN/*h*-BN (Figs. 3(g)-(i)) and as well as for H-graphene/*h*-BN and MoS_2/MoS_2 systems in Figs. S6, along the non-polar path I, the net positive charge on the upper layer and the negative charge in the bottom layer are uniformly distributed and relatively flat, which also corresponds to a small charge corrugation and sliding barrier. However, along the polar path II (Figs. 3(f) and (i)), electron-deficient and electron-rich atoms alternately appear in both the bottom and upper layers, which causes a large fluctuation of charge distribution along the sliding direction. Of course, the larger the

electronegativity difference, the larger the corrugation of charge distribution and friction. The charge density difference of H-graphene/*h*-BN and MoS_2/MoS_2 can be found in Fig. S7.

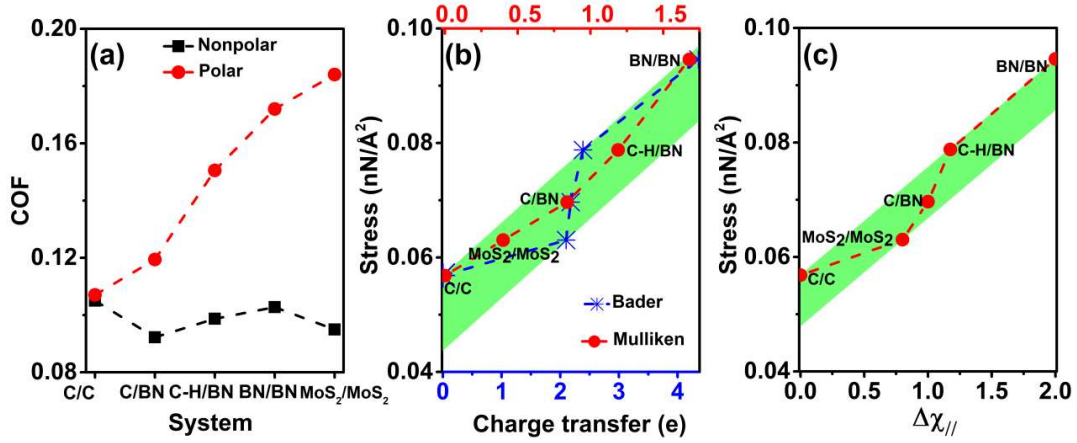

Fig. 4. Linear scaling law of friction. (a) Comparisons of COFs under the load of 0.7 nN/Å^2 among different bilayer systems. The shear stress as a function of (b) charge transfer and (c) electronegativity difference $\Delta\chi_{//}$.

To establish a clear relationship between electronegativity difference and interfacial friction, in Fig. 4 we compare the friction properties for all five calculated systems, as shown in Fig. 4(a). The comparisons of COF under the load of 0.7 nN/Å^2 in different systems shows that along the non-polar path I, the COFs are almost equal for all the systems, and about ~0.1, as typical vdW friction [5, 14, 15, 40, 41]. Note also that the polar path exhibits larger friction than for the non-polar path for all the systems.

To better understand the different COF along the polar direction II, we further extracted the functional relation between in-plane charge transfers and shear stress, as shown in Fig. 4 (b). As the different charge analysis methods may yield some deviation, the charge transfers were separately calculated by both the Mulliken and Bader charge analysis. Although the two methods provide a different amount of charge transfers, the change of charge transfer amount with respect to the friction force is quite similar, with errors falling within a small linear window. Interestingly, a linear functional relationship has been found between averaged frictional forces and the amount of intralayer charge transfer. Compared to the non-polar path I, the added friction in the polar path II can now be safely attributed to the enhanced charge density corrugation that appear in the polar path.

We define the systems total electronegativity difference along a path as

$\Delta\chi_{//} = |\chi_A - \chi_B| + |\chi_C - \chi_D|$, where χ_X represents electronegativity of the X atom (see Fig. 1(a)). By definition, the greater the electronegativity differences between its constituent atoms of each layer, the greater the $\Delta\chi_{//}$. Similar to charge transfer in Fig. 4(b), the frictional forces increase with the increase of $\Delta\chi_{//}$, which obeys a linear scaling law (Fig. 4(c)).

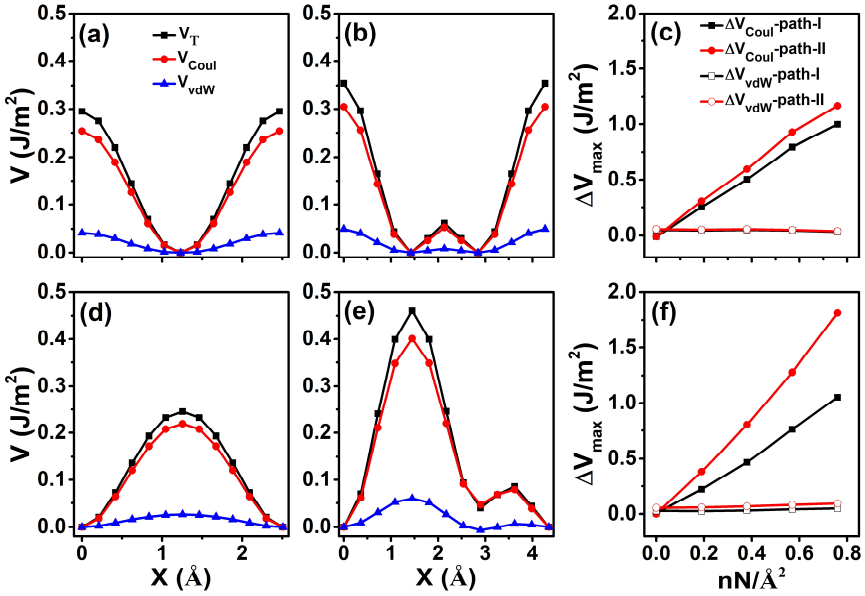

Fig. 5. Components of sliding energy barriers. The contributions of Coulomb interaction V_{Coul} and vdW energy V_{vdW} to total potentional energy V_{T} along (a) path I and (b) path II of graphene/graphene, (d) path I and (e) path II of *h*-BN/*h*-BN under the normal load of 0.2 nN/Å^2, and the minimum-energy value along each sliding path is set to 0. The difference of Coulomb interaction and vdW energy between the highest and lowest energy stackings as a function of normal load for (c) graphene/graphene and (f) *h*-BN/*h*-BN, respectively.

Finally, to see clearly which type of interactions plays the key role on electronegative friction in low dimensional systems, we further separately calculated the contributions of Coulomb interaction V_{Coul} and vdW dispersion force V_{vdW} to the total sliding energy barrier V_{T} along two sliding paths, as shown in Fig. 5. First of all, contrary to the traditional believe, instead of the vdW dispersion terms, the Coulomb interaction contributes to most of the sliding potential barrier. For the bilayer graphene system, the Coulomb contributions of the two paths are almost equal (see Fig. 5(a) and (b)), but for the bilayer *h*-BN system, the additional charge distribution induced by polarity enhances the Coulombic contribution to the friction on the polar path, which is almost twice that of

the non-polar path (see Fig. 5(d) and (e)). In addition, we calculated the relationship between the maximum energy barrier $\Delta V_{max} = V_{max} - V_{min}$, where V_{max} and V_{min} are the maximum and minimum of the protentional barrier V, and the normal load along the two sliding paths. Interestingly, the sliding barrier from vdW dispersion of about 0.01 J/m^2 is independent of the external normal load. However, the Coulomb contribution to sliding barrier increases with increasing pressure (see Fig. 5(c) and (f)). Therefore, it can be inferred that the interlayer friction of 2D layered materials is mainly determined by the Coulomb interaction. For non-polar paths, different 2D vdW materials exhibit similar small Coulomb barrier due to the smooth charge distribution, but for the polar path, the larger the polarity, and the larger charge distribution roughness and Coulomb barrier. The above results provide a full picture for the interlayer friction of 2D systems.

Discussion

The above analysis shows that the electronegativity difference in one preferred direction dominates the friction behavior along the sliding path for 2D systems. We denote this friction as electronegativity induced friction, which obeys a linear scaling law. It should be emphasized here that all the sliding interfaces in our calculation are commensurate. For elastically stiff 2D layers the polarity effect will be canceled for the incommensurate interface, such as identical double layers with relative rotation. However, if the effective elastic modulus is low enough commensurate-like domains may form, and the discussion above is relevant for these cases too.

In our previous studies, we proposed the charge roughness mechanism of nanofriction [8]. By comparing the tribological properties of graphene and hydrogenated graphene, we found that the coefficient of friction is proportional to the roughness of the charge distribution of the interface. In present work, we further show that the friction of the system is directly related to the corrugation of charge distribution in the sliding path by comparing the friction of different 2D systems. In polar systems, the electronegativity differences between component atoms can induce additional charge roughness, increasing the friction of the system.

To conclude, using the DFT with dispersion correction, the role of electronegativity in interfacial friction has been investigated. We have shown that these 2D systems exhibit almost the same friction along a nonpolar sliding path as the similar uniform charge distribution. In contrast, the interfacial friction force along the polar path is proportional to the electronegativity difference

among its constituent atoms. This linear scaling relationship between friction and electronegativity difference can be extended to other low-dimensional materials such as multiwall nanotubes and nanosheets [12], which will provide not only a new perspective in the field of tribology, but also a strategy for controlling friction at nanoscale.

Methods

Calculations details. Vienna Ab-initio Simulation Package (VASP) code, based on the Projector Augmented-Wave (PAW) method, was employed in the calculations (Ref. [18–20]). The exchange-correlation interactions were treated with the Generalized Gradient Approximation (GGA) of Perdew, Burke, and Ernzerhof (PBE), with a vdW correction determined by the Many-Body Dispersion (MBD) method (Ref. [21]). An energy cut-off of 600 eV and 21×21×1 Monkhorst-Pack grids were selected for the 2D irreducible Brillouin-Zone integration (Ref. [22]). The convergence thresholds for total energy and Hellmann-Feynman forces are 10^{-5} eV and 0.01 eV/Å, respectively. A vacuum space of at least 20 Å was set to avoid intercell interactions and the in-plane lattice constants of the bilayer structures were kept fixed.

Calculations of shear stress and coefficient of friction. The binding energy of the bilayer system is calculated by $E_{be} = E_{12} - E_1 - E_2$, where E_{12} is the total energy of the bilayer and E_1, E_2 are energies of the isolate single layers of the bilayer. At each position, the normal load F_N can be exerted on the bilayer system by setting its interlayer distances z according the function $F_N = -\partial E_{be}(z)/\partial z$. Thus, the potential energy at the position x under pressure F_N is $V(x, F_N) = E_{be}(x, z(x, F_N)) + F_N z(x, F_N)$. We define average friction force as $< F_f >= (V_{\max}(F_N) - V_{\min}(F_N))/\Delta x$, where $V_{\max}(F_N)$ and $V_{\min}(F_N)$ are the maximum and minimum of potential energy along one sliding path, and Δx is the distance between them. The coefficient of friction μ was calculated by $\mu = < F_f > / F_N$, and the shear stress $\tau = < F_f > / A$ is the average friction force divided by the surface area A [23].

Calculations of charge density difference. The charge density difference is calculated by $\Delta\rho = \rho_{AB} - \rho_A - \rho_B$. Here two kinds of charge density difference were calculated, one is charge transfer between atoms in single layers, $\Delta\rho = \rho_{AB} - \rho_A - \rho_B$, ρ_{AB}, ρ_A and ρ_B are the charge

densities of single layer, free A and B atoms, respectively. Another is the charge transfer between layers in the systems, $\Delta\rho = \rho_{L_1L_2} - \rho_{L_1} - \rho_{L_2}$, where $\rho_{L_1L_2}$, ρ_{L_1} and ρ_{L_2} are the charge densities of bilayer layer, top layer L_1 and bottom layer L_2, respectively.

Data availability. The data that support the findings of this study are available from the corresponding authors on request.

References

[1] Urbakh, M. & Meyer, E. The renaissance of friction. *Nat. Mater.* **9**, 8–10, (2010).

[2] Braun, O. M. & Naumovets, A. G. Nanotribology: Microscopic mechanisms of friction. *Surf. Sci. Rep.* **60**, 79–158 (2006).

[3] Lee, C., Li, Q., Kalb, W., Liu, X., Berger, H., Carpick R. W. & Hone, J. Frictional characteristics of atomically thin sheets. *Science* **328**, 76 (2010).

[4] Spear, J. C. B., Ewers, W. & Batteas, J. D. 2D-nanomaterials for controlling friction and wear at interfaces. *Nano Today* **10**, 301–314 (2015).

[5] Cahangirov, S., Ataca, C., Topsakal, M., Sahin H. & Ciraci, S. Frictional figures of merit for single layered nanostructures. *Phys. Rev. Lett.* **108**, 126103 (2012).

[6] Hod, O., Meyer, E., Zheng, Q. & Urbakh, M. Structural superlubricity and ultralow friction across the length scales. *Nature* **563**, 485–492 (2018).

[7] Sinclair, R. C., Suter, J. L. & Coveney, P. V. Graphene–graphene interactions: Friction, superlubricity, and exfoliation. *Adv. Mater*. **30**, 1–7 (2018).

[8] Wang, J., Li, J., Fang, L., Sun, Q. & Jia, Y. Charge distribution view: Large difference in friction performance between graphene and hydrogenated graphene systems. *Tribol. Lett*. **55**, 405 (2014).

[9] Wolloch, M., Levita, G., Restuccia P. & Righi, M. C. Interfacial charge density and its connection to adhesion and frictional forces. *Phys. Rev. Lett.* **121**, 026804 (2018).

[10] Wolter, B., Yoshida, Y., Kubetzka, A., Hla, S.–W., Bergmann K. v. & Wiesendanger, R. Spin friction observed on the atomic scale. *Phys. Rev. Lett.* **109**, 116102 (2012).

[11] Sanderson, R. T. Electronegativity and bond energy. *J. Am. Chem. Soc*. **105**, 2259–2261 (1983).

[12] Niguès, A., Siria, A., Vincent, P., Poncharal, P. & Bocquet, L. Ultrahigh interlayer friction in multiwalled boron nitride nanotubes. *Nat. Mater.* **13**, 688–693 (2014).

[13] Tocci, G., Joly, L. & Michaelides, A. Friction of water on graphene and hexagonal boron nitride from Ab initio methods: Very different slippage despite very similar interface structures. *Nano Lett*. **14**, 6872–6877 (2014).

[14] Marom, N., Bernstein, J., Garel, J., Tkatchenko, A., Joselevich, E., Kronik, L. & Hod, O. Stacking and registry effects in layered materials: The case of hexagonal boron nitride. *Phys. Rev. Lett.* **105**, 046801 (2010).

[15] Hod, O. Graphite and hexagonal boron-nitride have the same interlayer distance. Why? *J. Chem. Theory Comput*. **8**, 1360–1369 (2012).

[16] Gao, W. & Tkatchenko, A. Sliding mechanisms in multilayered hexagonal boron nitride and graphene: The effects of directionality, thickness, and sliding constraints. *Phys. Rev. Lett*. **114**, 096101 (2015).

[17] Falin, A., Cai, Q. R., Santos, E. J. G., Scullion, D., Qian, D., Zhang, R., Yang, Z., Huang, S., Watanabe, K., Taniguchi, T., Barnett, M. R., Chen, Y., Ruoff, R. S. & Li, L. H. Mechanical properties of atomically thin boron nitride and the role of interlayer interactions. *Nat. Commun.* **8**, 15815 (2017).

[18] Kresse, G. & Furthmüller, J. Efficient iterative schemes for ab initio total–energy calculations using a plane-wave basis set. *Phys. Rev. B* **54**, 11169 (1996).

[19] Kresse, G. & Furthmüller, J. Efficiency of ab–initio total energy calculations for metals and semiconductors using a plane–wave basis set. *Comput. Mater. Sci*. **6**, 15 (1996).

[20] Blöchl, P. E. Projector augmented-wave method. *Phys. Rev. B* **1994**, *50*, 17953.

[21] Tkatchenko, A., DiStasio R. A. Jr., Car R. & Scheffler, M. Accurate and efficient method for many–body van der Waals interactions. *Phys. Rev. Lett.* **108**, 236402 (2012).

[22] Monkhorst, H. J. & Pack, J. D. Special points for Brillouin–zone integretions. *Phys. Rev. B* **13**, 5188 (1976).

[23] Zhong, W. & Tománek, D. First-principles theory of atomic–scale friction. *Phys. Rev. Lett.* **64**, 3054 (1990).

[24] Zilibotti, G. & Righi, M. C. Ab initio calculation of the adhesion and ideal shear strength of planar diamond interfaces with different atomic structure and hydrogen coverage. *Langmuir* **27,** 6862–6867 (2011).

[25] Constantinescu, G., Kuc A. & Heine, T. Stacking in bulk and bilayer hexagonal boron nitride. *Phys. Rev. Lett*. **111**, 036104 (2013).

[26] Sheehan, P. E. & Lieber, C. M. Nanotribology and nanofabrication of MoO_3 structures by atomic force microscopy. *Science* **272**, 1159 (1996).

[27] Balakrishna, S. G., de Wijn, A. S. & Bennewitz, R. Preferential sliding directions on graphite. *Phys. Rev. B* **89**, 245440 (2014).

[28] Wang, W., Shen, J. & He, Q.–C. Microscale superlubricity of graphite under various twist angles. *Phys. Rev. B* **99**, 054103 (2019).

[29] Diestler, D. J., Rajasekaran, E. & Zeng, X. C. Static frictional forces at crystalline interfaces. *J. Phys. Chem. B* **101**, 4992–4997 (2007).

[30] Vazirisereshk, M. R., Ye, H., Ye, Z., Otero-de-la-Roza, A., Zhao, M.–Q., Gao, Z., Johnson, A. T. C., Johnson, E. R., Carpick R. W. & Martini, A. Origin of nanoscale friction contrast between supported graphene, MoS_2, and a Graphene/MoS_2 heterostructure. *Nano Lett.* **19**, 5496–5505 (2019).

[31] Persson, B. N. J. Comment on "On the origin of frictional energy dissipation". *Tribol. Lett.* **68**, 28 (2020).

[32] He, J., Hummer K. & Franchini, C. Stacking effects on the electronic and optical properties of bilayer transition metal dichalcogenides MoS_2, $MoSe_2$, WS_2, and WSe_2. *Phys. Rev. B* **89**, 075409 (2014).

[33] Wen, M., Carr, S., Fang, S., Kaxiras, E. & Tadmor, E. B. Dihedral–angle–corrected registry–dependent interlayer potential for multilayer graphene structures. *Phys. Rev. B* **98**, 235404 (2018).

[34] Lebedeva, I. V., Lebedev, A. V., Popov, A. M. & Knizhnik, A. A. Comparison of performance of van der Waals–corrected exchange–correlation functionals for interlayer interaction in graphene and hexagonal boron nitride. *Comp. Mater. Sci*. **128**, 45–58 (2017).

[35] Popov, A. M., Lebedeva, I. V., Knizhnik, A. A., Lozovik, Y. E. & Potapkin, B. V. Barriers to motion and rotation of graphene layers based on measurements of shear mode frequencies. *Chem. Phys. Lett*. **536**, 82–86 (2012).

[36] Tan, P. H., Han, W. P., Zhao, W. J., Wu, Z. H., Chang, K., Wang, H., Wang, Y. F., Bonini, N., Marzari, N., Pugno, N., Savini, G., Lombardo A. & Ferrari, A. C. The shear mode of multilayer graphene. *Nature Mater*. **11**, 294 (2012).

[37] Baskin, Y. & Meyer, L. Lattice constants of graphite at low temperatures. *Phys. Rev. B* **100**, 544 (1955).

[38] Zacharia, R., Ulbricht, H. & Hertel, T. Interlayer cohesive energy of graphite from thermal desorption of polyaromatic hydrocarbons. *Phys. Rev. B* **69**, 155406 (2004).

[39] Warner, J. H., Rümmeli, M. H., Bachmatiuk, A. & Büchner, B. Atomic resolution imaging and topography of boron nitride sheets produced by chemical exfoliation. *ACS Nano* **4***,* 1299–1304 (2010).

[40] Zhou, S., Han, J., Dai, S., Sun, J. & Srolovitz, D. J. van der Waals bilayer energetics: Generalized stacking-fault energy of graphene, boron nitride, and graphene/boron nitride bilayers. *Phys. Rev. B* **92**, 155438 (2015).

[41] Li, B., Yin, J., Liu, X., Wu, H., Li, J., Li, X. & Guo, W. Probing van der Waals interactions at two-dimensional heterointerfaces. *Nat. Nanotech*. **14**, 567–572 (2019).

Acknowledgements

The work was supported by the National Natural Science Foundation of China (Grant No. U1604131, 11774078, 11805295).

Author contributions

Y. Jia conceived the project. J. Wang performed the simulations. J. Wang, Y. Jia and B. N. J. Persson analyzed the obtained results. J. Wang, A. Tiwari, B. N. J. Persson, and Y. Jia wrote the paper. All the authors commented on the manuscript.

Competing interests

The authors declare no competing interests.

Supplementary Files

This is a list of supplementary files associated with this preprint. Click to download.

- SupportInformation.pdf